Structural tuning of magnetism in the orthorhombic perovskite $Nd_{1-x}Y_xMnO_3$: Evidence for magnetic phase separation

S. Landsgesell,[1] A. Maljuk,[1] T. C. Hansen,[2] O. Prokhnenko,[1] N. Aliouane,[1,3] and D. N. Argyriou[1,*]
[1]*Helmholtz-Zentrum Berlin für Materialien und Energie, Glienicker Str. 100, D-14109 Berlin, Germany*
[2]*Institute Laue-Langevin, 6 Rue Jules Horowitz, F-38042 Grenoble, France*
[3]*Institute for Energy Technology, P.O. Box 40, NO-2027 Kjeller, Norway*
(Received 30 March 2009; revised manuscript received 5 June 2009; published 9 July 2009)

We report on the magnetic and structural properties of the perovskite solid solution $Nd_{1-x}Y_xMnO_3$, using magnetization and neutron powder-diffraction measurements. The orthorhombic perovskite structure (*Pbnm*) is obtained over the composition range of $0 \leq x \leq 0.6$. The Mn-O-Mn bond angles and the Néel temperature T_N decrease with increasing x and track closely similar behavior established for the general series of manganites $RMnO_3$ (R=rare earth). For lower doped samples, the antiferromagnetic A-type Mn order is stable, while for higher doping the diffraction data can be modeled using an incommensurate spin-density-wave (SDW) model. In both cases, we find that Mn spins are aligned along the b axis. For intermediate compositions $0.4 \leq x < 0.55$, we find a coexistence of A-type and SDW magnetic order. On symmetry grounds, we argue that these two magnetic phases cannot occupy the same volume but rather this coexistence region is indicative of a notable *magnetic phase separation*.

DOI: 10.1103/PhysRevB.80.014412 PACS number(s): 75.25.+z, 74.62.Bf, 75.30.Fv, 75.30.Kz

I. INTRODUCTION

Perovskite manganites are of interest due to the variety of strongly correlated electron phenomena they exhibit such as colossal magnetoresistance, charge and orbital ordering, and electronic phase separation.[1,2] Such complex behavior arises from competing interactions that influence the magnetic, electronic, and structural properties. In charge doped manganites, holes are introduced by chemical substitution of the trivalent lanthanide for a divalent cation (as, for example, in $La_{1-x}Ca_xMnO_3$). With increasing doping, antiferromagnetic (AFM) superexchange and ferromagnetic (FM) double exchange compete in a complex energy landscape to form an extremely rich electronic and magnetic phase diagram.[1,2]

More recently, however, a detailed investigation of the insulating $RMnO_3$ (R is a trivalent rare-earth ion) has revealed a new way to tune magnetic interactions and properties in manganites. In $LaMnO_3$, the antiferrotype ordering of singly-occupied Mn^{3+} $3d_{3x^2-r^2}$ and $3d_{3y^2-r^2}$ orbitals produces ferromagnetic interactions within the *ab* plane of the perovskite lattice, while the coupling between planes is antiferromagnetic.[3] This ordering is known as A-type [Fig. 1(a)] and is stabilized by ferromagnetic nearest-neighbor interactions (J_1), while the next-nearest-neighbor interaction (J_2) is weak but also ferromagnetic. By decreasing the size of the R ions, the A-type ordering becomes frustrated as indicated by the steady decrease in T_N from 150 K for R=La to ~40 K for R=Eu.[4] Accompanying this decreases in T_N is a sterically driven decrease in the Mn-O-Mn bond angles, progressively weakening the FM J_1 interaction and rendering the J_2 interaction antiferromagnetic due to a significant overlap between adjacent e_g orbitals.[5–8] Indeed, $HoMnO_3$, exhibits a commensurate AFM ordering within the *ab* plane with both FM and AFM nearest-neighbor interactions (E-type phase).[9]

For compounds in the intermediate region between A and E types, with R=Gd, Tb, and Dy,[10,11] commensurate AFM ordering is not stable and the competition between J_1 and J_2 leads to an incommensurate cycloidal magnetic structure whose most prominent feature is the breaking of inversion symmetry.[7] Although the size of the polarization is relatively small (~800 $\mu C/m^2$ for $TbMnO_3$) compared to proper ferroelectrics, this new way of generating a strong magnetoelectric coupling leads to materials where the ferroelectric polarization can be controlled directly by a magnetic field.[12] For R=Tb and Dy, the direction of the ferroelectric polarization can be flopped from the c axis to the a axis with magnetic field applied along the a and b directions,[12,13] while for R=Gd ferroelectricity can be induced with a magnetic field

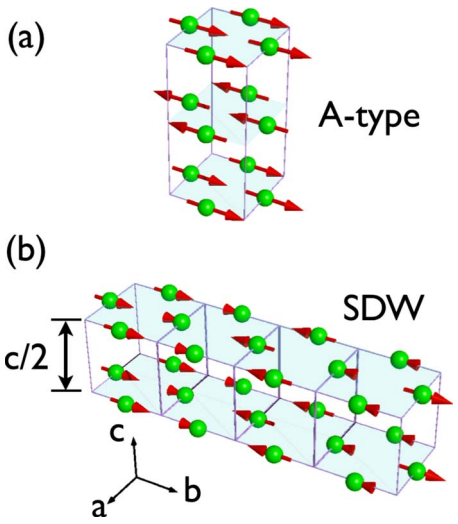

FIG. 1. (Color online) (a) The A-type antiferromagnetic ordering of Mn spins as found in $NdMnO_3$. As determined from the NPD data, Mn spins point along the b axis. The orthorhombic unit cell is shown, while Mn atoms are represented as spheres. (b) The incommensurate magnetic ordering of Mn spins in the form of a collinear spin-density wave propagating along the b axis found for compositions of $0.4 \leq x \leq 0.6$. The shown periodicity here is q=0.25.

TABLE I. List of the samples, preparation conditions, magnetic remanence, and effective moment. Samples were prepared by SSRs in either N_2 or in air and by the optical FZ method in Ar atmosphere. Ferromagnetic remanence and moments were determined by isothermal magnetic hysteresis measurements at 5 K, while the effective moment was determined using the temperature-dependent magnetization. Néel temperatures (T_N) determined from magnetization [$\chi(T)$] and temperature-dependent NPD measurements are also given.

x	Preparation method	Remanence (emu/mol)	Moment ($\frac{\mu_B}{\text{f.u.}}$)	T_N [$\chi(T)$] (K)	T_N (NPD) (K)
0.0	SSR in N_2	7.7	1.38	88	
0.1	SSR in N_2	5.7	1.02	83	
0.2	SSR in N_2	4.8	0.86	75	
0.3	SSR in air	3.7	0.66	63	
0.35	SSR in air	2.8	0.50	56	57
0.4	FZ in Ar	2.1	0.38	54	55
0.45	FZ in Ar	1.8	0.32	53	52
0.5	FZ in Ar	0.6	0.10	52	51
0.6	FZ in Ar			50	49

applied parallel to the *b* axis.[10] Also the *E*-type structure has been proposed to be ferroelectric on the basis of the exchange striction and, indeed, some recent reports confirm this prediction.[14,15]

Although the suppression of the collinear *A*-type antiferromagnetic ordering in favor of the cycloidal order for R =Tb and Dy is evident, the exact details of how one magnetic structure develops into the other are not entirely clear. For example, is the transition from the *A*-type to the cycloidal ordering with decreasing R size on the first or on the second order? Ideally, one would perform neutron-diffraction experiments to probe the magnetic ordering directly; however, the high neutron absorption cross section of Sm, Eu, and Gd, which make up compositions in the cross-over region from the *A* type to incommensurate magnetic order, prohibit such experiments. While the solid solution of $Eu_{1-x}Y_xMnO_3$ has been examined, detailed neutron-scattering experiments are prohibitive for low Y doping.

In this paper, we report on the synthesis, crystal, and magnetic structures of the solid solution $Nd_{1-x}Y_xMnO_3$. We find that we can synthesize phase-pure samples over the composition region $0<x<0.6$ using either solid-state reactions (SSRs) or floating-zone (FZ) image furnace methods. Analysis of neutron powder-diffraction (NPD) data shows that with increasing x, the Mn-O bond lengths remain essentially unchanged but the Mn-O-Mn bond angles that control the strength and sign of superexchange interactions vary from 149° to 146°. The magnetic phase diagram of this solid solution tracks well that of the $RMnO_3$ manganites. With increasing x, we find that T_N for the *A*-type antiferromagnetic phase decreases rapidly up to $x\sim0.4$. Between $0.35<x<0.55$, we find a region of coexistence between *A*-type magnetic ordering and an incommensurate spin-density wave (SDW), while for $x=0.60$ we observe only the SDW phase. In this series of materials, we find that the Nd^{3+} ions order ferromagnetically; however, the size of the ferromagnetic moment decreases linearly with x as the R site is diluted by nonmagnetic Y^{3+} ions.

II. EXPERIMENTAL

Single phase samples of $Nd_{1-x}Y_xMnO_3$ with $x=0.0$, 0.1, 0.2, 0.3, and 0.35 were prepared by standard solid-state reaction techniques using dry and phase-pure precursors of Nd_2O_3, Y_2O_3, and Mn_2O_3 with purity >99.99%. Stoichiometric quantities of precursors were mixed and annealed at 1400 °C for 24 h with intermediate grindings. Samples with $x=0.0,0.1,0.2$ were prepared under nitrogen atmosphere to prevent the oxidation of Mn^{3+} to Mn^{4+}.[16] Samples with x =0.3 and 0.35 were prepared in air to stabilize the orthorhombic phase and suppress the occurrence of the hexagonal manganite phase preferred for Y rich compositions.[17] In addition, samples with $x=0.4$, 0.45, 0.5, and 0.6 were prepared under a pressure of 8 bar of argon in a floating-zone image furnace by recrystallizing stoichiometric ceramic rods with diameter of approximately 8 mm. Crystalline boules from these experiments were crushed and ground to fine powder for diffraction measurements and for physical properties measurements. A short overview of the samples and their preparation method is shown in Table I.

Phase purity in all samples was checked by the x-ray diffraction (XRD) using a Bruker D8 advance reflection mode x-ray diffractometer. Magnetic-susceptibility measurements were performed using a Quantum Design superconducting quantum interference device (SQUID) magnetometer with a dc field of 5000 Oe from 2 to 200 K. We used approximately 100 mg powder samples, with cooling in zero field, measuring field of 5000 Oe, and a heating rate of 1 K/min. Magnetic hysteresis measurements were done at 5 and 85 K, performing a full hysteresis loop between 5 and −5 T starting from zero field with 1000 Oe steps. NPD data were measured at 2 and 300 K for samples $x=0.0-0.3$ using the high-resolution neutron powder diffractometer E9 with a wavelength of λ =1.797 Å operated at the BENSC facility of the Helmholtz-Zentrum Berlin. Temperature-dependent diffraction scans, between 2 and 300 K were carried out for $x=0.35-0.6$ on the D20 neutron powder diffractometer[18] at the Institut Laue

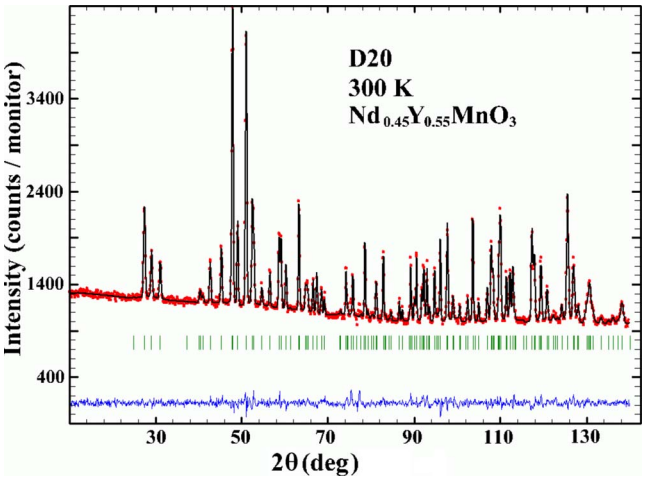

FIG. 2. (Color online) A typical Rietveld analysis of the NPD data. The NPD data (circles) were measured from the $x=0.45$ sample at 300 K using the E9 diffractometer. The upper solid line represents the calculated NPD pattern and the lower solid line represents the difference between measured and calculated patterns. The vertical tick marks represents allowed reflections for the *Pbnm* space group.

Langevin from 2 to 150 K in a high-resolution mode using a neutron wavelength of $\lambda=1.869\,9$ Å. All NPD data were analyzed by the Rietveld method using the FULLPROF suite of programs.[19,20]

III. RESULTS

A. Room-temperature crystal structure

Both XRD and NPD data measured at 300 K were consistent with an orthorhombically distorted perovskite structure with space group *Pbnm* (No. 62). In Fig. 2, we show a representative Rietveld fit to the NPD data measured at 300 K from the $x=0.45$ sample, while in Table II we report relevant crystallographic parameters at 300 K for all samples. As is evident from Table II, changes in lattice constants are consistent with Vegard's law indicating that the substitution of Y for Nd results in a solid solution. Indeed, a careful examination of peak profiles of the NPD data gave no indication of the presence of two orthorhombic phases indicative of chemical phase separation or a miscibility gap. The values of the full width at half maximum from the NPD data were close to those expected from the instrumental resolution function and allowed us to place an upper limit to any possible chemical phase separation to $\Delta x<0.05$.

While diffraction data from all samples could be modeled using a single phase orthorhombic perovskite phase, measurements of the $x=0.5$ and 0.6 samples showed small traces of the hexagonal manganite phase (0.9 wt % and 1.4 wt %, respectively). This observation indicates that the orthorhombic to hexagonal phase boundary is located approximately around $x\sim0.55$ and varies with preparation conditions. Indeed, we were not able to synthesize phase-pure samples with $x>0.6$, and the best results in this high x region were for samples prepared by the floating-zone method. The behavior we find here is similar to that found in the $Eu_{1-x}Y_xMnO_3$ solid solution where this phase boundary occurs at $x\sim0.7$.[21] In general, all three lattice constants decrease with increasing x reflecting the smaller size of the Y^{3+} ion substituted for the larger Nd^{3+}.

The difference of the ionic size between Nd^{3+} and Y^{3+} is significant (98 pm and 90 pm, respectively) with the ionic variance reaching a maximum at $x=0.5$ and the unit-cell volume and lattice constants decreasing with tolerance factor and mean ionic radii $\langle r_A\rangle$ of the R site. If we scale composition x to $\langle r_A\rangle$, then the $x=0.4$ sample has the same $\langle r_A\rangle$ as $EuMnO_3$. However, the volume and the lattice constants

TABLE II. Room-temperature structural parameters and R factors determined from the Rietveld analysis of the NPD data. The atomic sites are Mn^{3+} at $4b(1/200)$, Nd^{3+}/Y^{3+} at $4c(xy3/4)$, and the O^{2-} atoms (O1 and O2) at $4c(xy1/4)$ and $8d(xyz)$.

x	a (Å)	b (Å)	c (Å)	x (Nd/Y)	y (Nd/Y)	x (O1)	y (O1)	x (O2)	y (O2)	z (O2)	χ^2
Polycrystalline (N_2)											
0	5.4146 (3)	5.8472 (3)	7.5445 (4)	−0.0141(7)	0.0708 (6)	0.0901 (7)	0.4735 (7)	0.7147 (6)	0.3167 (6)	0.0478 (6)	1.90
0.1	5.4006 (3)	5.8544 (3)	7.5280 (4)	−0.0142(9)	0.0714 (8)	0.0917 (9)	0.4721 (8)	0.7144 (8)	0.3189 (8)	0.0476 (8)	2.02
0.2	5.3955 (2)	5.8533 (2)	7.5120 (2)	−0.0143(7)	0.0736 (7)	0.0938 (7)	0.4720 (7)	0.7127 (6)	0.3204 (6)	0.0477 (6)	2.30
Polycrystalline (air)											
0.3	5.3587 (4)	5.8226 (4)	7.4841 (4)	−0.0137(7)	0.0757 (7)	0.0911 (7)	0.4735 (8)	0.7065 (7)	0.3228 (6)	0.0481 (6)	2.86
0.35	5.3540 (3)	5.8319 (3)	7.4771 (4)	−0.0139(8)	0.0768 (8)	0.0924 (8)	0.4744 (7)	0.7056 (7)	0.3230 (7)	0.0483 (7)	2.24
Crystalline samples											
0.4	5.3549 (3)	5.8624 (3)	7.4666 (4)	−0.0152(7)	0.0768 (7)	0.0958 (7)	0.4711 (6)	0.7087 (6)	0.3233 (6)	0.0488 (6)	3.39
0.45	5.3428 (3)	5.8617 (3)	7.4530 (4)	−0.0154(6)	0.0778 (6)	0.0976 (6)	0.4703 (6)	0.7074 (5)	0.3244 (5)	0.0490 (5)	2.24
0.5	5.3436 (3)	5.8639 (3)	7.4542 (4)	−0.0157(9)	0.0788 (9)	0.0991 (9)	0.4708 (8)	0.7065 (8)	0.3246 (8)	0.0491 (8)	6.8
0.6	5.3275 (2)	5.8607 (2)	7.4370 (3)	−0.0166(9)	0.0806 (9)	0.1015 (9)	0.4688 (8)	0.7046 (8)	0.3258 (8)	0.0498 (8)	8.7

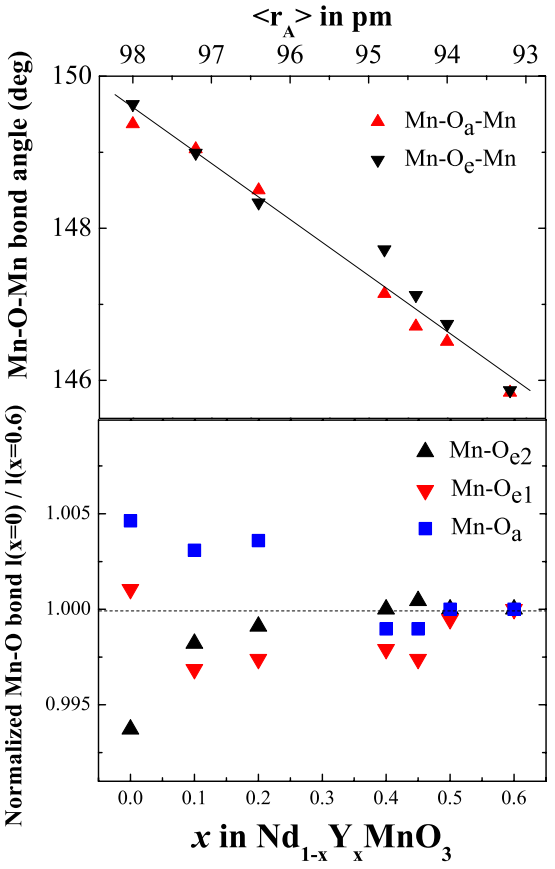

FIG. 3. (Color online) Variation in the Mn-O-Mn angles (upper frame) and the three Mn-O distances (lower frame) with x (lower x axis) and mean ionic radii $\langle r_A \rangle$ in the solid solution $Nd_{1-x}Y_xMnO_3$. The Mn-O bond lengths are normalized to those determined for $x=0.6$. In this orthorhombic perovskite, there are three Mn-O bond lengths and two Mn-O-Mn angles. The subscripts "e" and "a" denote equatorial and apical bond lengths and angles, respectively. Error bars are smaller or equal in the magnitude to the size of the symbols.

match those of $x=0.5$. Also the same behavior is found for $SmMnO_3$ where the $x=0.25$ sample has the same $\langle r_A \rangle$, but its volume matches that for $x=0.35$. This is indicative for a systematic departure from the trends established for the $RMnO_3$ series, as was noted also for $Eu_{1-x}Y_xMnO_3$,[21] and we speculate that it may be related to the size mismatch of Nd and Y ions.

In Fig. 3, we plot the variation in the ⟨Mn-O-Mn⟩ bond angles and ⟨Mn-O⟩ bond lengths as a function of x determined from the NPD data. The ⟨Mn-O⟩ bond lengths show an almost negligible dependence on x, a result that is not surprising considering that they are sensitive to the Mn^{3+} oxidation state which remains unchanged for this series of compounds. Indeed, the 300 K NPD data are consistent with the orbital ordering of Mn^{3+} $3d_{3x^2-r^2}$ and $3d_{3y^2-r^2}$ orbitals as found in $LaMnO_3$.[3] On the other hand, we find a considerable dependence of the Mn-O-Mn bond angle on x; it decreases linearly from 149.0(1)° to 146.1(1)° as x is varied from 0 to 0.6 and reflects the decrease in $\langle r_A \rangle$. Indeed in the $RMnO_3$ manganites, a similar trend is found with decreasing r_A. As R is varied from Nd through to Tb, the ⟨Mn-O-Mn⟩ bond angle varies from 149° to 143°, and r_A varies over a similar range as we have here in the $Nd_{1-x}Y_xMnO_3$ solid solution (i.e., from 98 pm for Nd^{3+} to 92 pm for Tb^{3+}).[5]

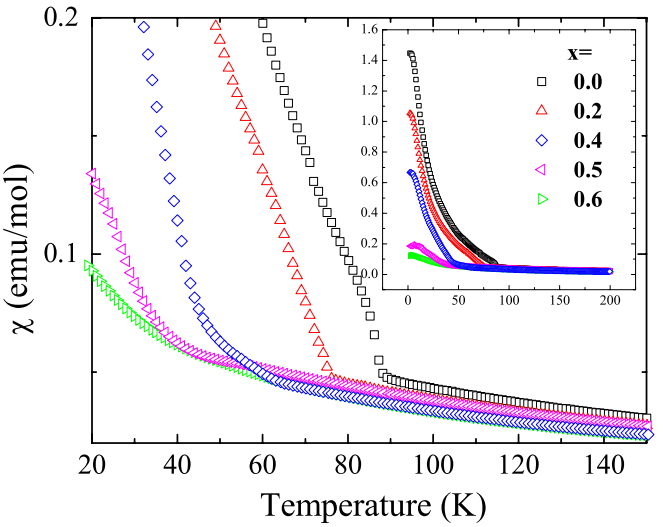

FIG. 4. (Color online) Temperature-dependent dc magnetization measurements from samples $x=0.0$, 0.2, 0.4, 0.5, and 0.6 performed using a field of 5000 Oe. The dc magnetization measurements for the remaining samples are not shown for clarity but follow the same trends as indicated by the data shown.

B. Magnetic properties

We first turn our attention to the $x=0$ sample. The magnetization data shown in Fig. 4 show a sharp up turn at 87 K, a behavior that is not expected for AFM ordering, neither reminiscent of a second-order phase transition; although the onset of this feature is consistent with the value of T_N from previous reports.[22,23] The magnetization data, however, are reminiscent of an induced FM transition likely arising from the ordering of Nd^{3+} spins.[22,23] As discussed elsewhere,[22,24] the A-type order of the Mn^{3+} spins exhibits a non-negligible antisymmetric component leading to a small FM component perpendicular to the sheets (i.e., $H \| c$). Therefore, the A-type ordering of Mn spins can likely induce the FM ordering of Nd^{3+} spins. As a result, T_N and T_C are at the same temperature and the rise of the magnetization curve should be indicative of T_N. This assumption is confirmed by our neutron-diffraction measurements described below, where we find the Mn spins order with A-type structure and Nd spins order ferromagnetically along the c axis. The FM ordering of Nd spins is also reflected in hysteresis curves measured at 5 K (see Fig. 5). Here we find a behavior typical for a weak ferromagnet for the $x=0$ sample, with a coercivity of lower than 1000 Oe and a small but measurable remanence, while hysteresis loops measured at 85 K were consistent with paramagnetism. With increasing x, the strength of the coercive field is approximately the same for all samples but the remanence field and saturation (FM) moment decreases with x as indicated in Table I. For $x=0.6$, we do not obtain a ferromagnetic hysteresis loop, indicating that for this composition there is no significant ferromagnetic contribution to the mag-

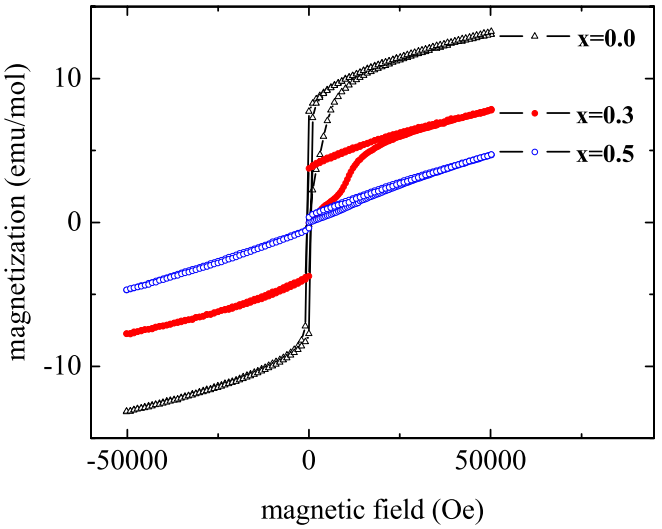

FIG. 5. (Color online) Hysteresis curves measured with dc SQUID magnetometer at 5 K on samples $x=0.0$, 0.3, and 0.5.

netic ordering. The susceptibility measurements from all samples followed a Curie-Weiss behavior above T_N, giving Curie constants that decrease with increasing x and vary from $\mu_{\text{eff}}=5.8$ to $5.4\mu_B$, somewhat lower than the expected values of $\mu_{\text{eff}}=6.1$ to $5.7\mu_B$.

The magnetization data show that with decreasing x, the onset temperature of the magnetic ordering also decreases, from $T_N=88$ to 49 K as x is varied from 0 to 0.6. Here, the values of T_N or T_C were determined by taking the derivative of $M(T)$ and are given in Table I. The overall behavior of the $Nd_{1-x}Y_xMnO_3$ solid solution, therefore, appears to track that of the $RMnO_3$ perovskite manganites where T_N is reduced as the size of the rare-earth ion is decreased.[5]

C. Magnetic structure

In this section, we present temperature-dependent NPD measurements used to characterize the magnetic ordering of the $Nd_{1-x}Y_xMnO_3$ solid solution. Data were measured on warming from 2 to ~120 K for $x=0.35$ to 0.6 samples using the D20 diffractometer, while further data were measured at 2 K for $x=0.0$ to 0.3 samples on the E9 diffractometer. From the temperature dependence of magnetic intensities, we were able to determine T_N independently and compare these values to the magnetization measurements. We found excellent agreement as illustrated by the example scan for the $x=0.4$ sample shown in Fig. 6 and in Table I. More importantly for the $x\leq 0.3$ samples, the quality of the Rietveld analysis could be improved significantly by the addition of a ferromagnetic ordering for the Nd^{3+} ions for samples with $x=0$ to 0.3 as shown in Fig. 7, confirming the conclusions of the magnetization measurements. The largest ferromagnetic contribution is observed for the $x=0$ sample where we find a Nd^{3+} spin ordering along the c axis with a moment of $1.5\mu_B$/Nd. As x increases, the magnitude of the Nd^{3+} moment steadily decreases as displayed in Fig. 9, while for $x>0.3$ we find no evidence of ferromagnetic Nd^{3+} ordering in the NPD data. The Rietveld analysis of the NPD data for $x\leq 0.2$ compositions indicate that Mn spins are collinear and oriented along the b axis ($R_w=6.0\%$ for moment parallel to b axis ($m\|b$) compared to $R_w=8.2\%$ for $m\|a$ or $R_w=11.9\%$ for $m\|c$.

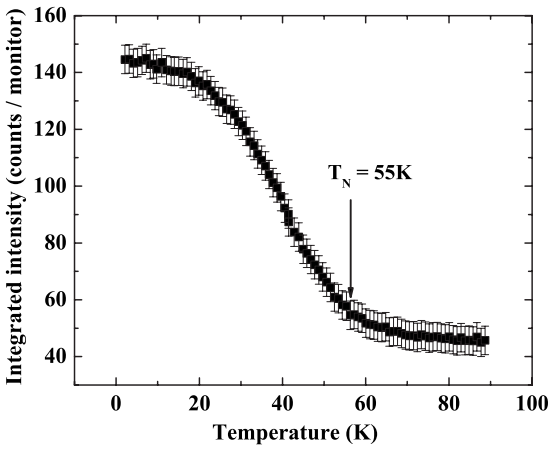

FIG. 6. Temperature dependence of the integrated intensity of the (001) magnetic reflection indicative of A-type AFM ordering. These NPD data were measured from the $x=0.4$ sample using the D20 diffractometer. T_N as indicated by these data is shown and agrees well with the value of 54 K determined from the magnetization data. For the NPD data, T_N was taken as the temperature at which magnetic Bragg peaks disappeared on warming.

For higher x compositions, we observe a series of incommensurate magnetic reflections below T_N in addition to the A-type magnetic Bragg peaks. These incommensurate reflections can be indexed with a magnetic propagation vector of $k=q\mathbf{b}^*$ with $q=\{0.23,\ldots,0.27\}$. This change in magnetic order with x is illustrated in Fig. 8 where we show NPD data

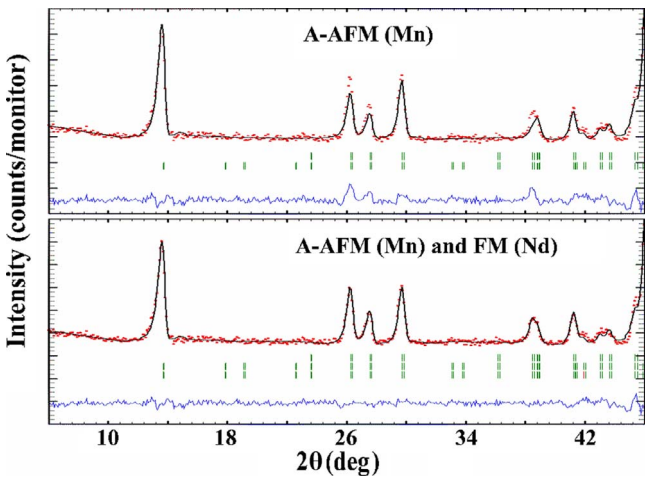

FIG. 7. (Color online) Rietveld analysis of the NPD data measured from $NdMnO_3$ at 2 K using the E9 diffractometer in Berlin displayed over the region of $2\theta=6$ to 46. In the upper panel the data are modeled assuming an A-type ordering for Mn spins only. This model of nuclear and magnetic structures leads to a deficiency in the intensity of reflections between 26° and 29°. In the lower panel results of an analysis using the same model as above with the addition of a FM Nd-spin component along the c axis. This model yields a magnetic moments of $4.1\mu_B$ and $1.5\mu_B$ per formula unit for the Mn and Nd ions, respectively.

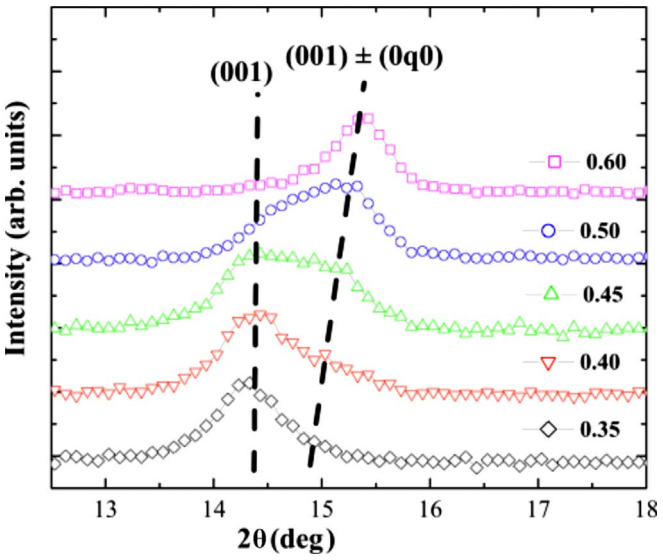

FIG. 8. (Color online) Portion of the NPD data measured on D20, showing the AFM (001) *A*-type reflection and the incommensurate SDW reflection $(001)\pm(0,q,0)$ for various samples measured at 2 K.

measured over the angular region $2\theta=12,\ldots,18$ at 2 K for compositions $x=0.35$ to 0.6. This angular range covers the region where the commensurate (001) reflection indicative of *A*-type order and the incommensurate $(001)\pm k$ reflection are observed. For the $x=0.35$ sample, a single (001) reflection is found; however, for increasing x there is an additional reflection that appears at slightly higher angles and for $x=0.6$ only this incommensurate reflection is observed. For the intermediate compositions $0.4\leq x\leq 0.5$, the intensity ratio of these two reflections varies, favoring the incommensurate peak as x increases. A notable feature of these data is that for $x=0.4$ the incommensurate reflection appears broader than the commensurate (001) peak, while in the $x=0.5$ sample the reverse behavior may be occurring, and for the $x=0.6$ sample the incommensurate reflection is as sharp as the (001) peak in the $x=0.35$ sample. This may indicate that the coherence length of these two different magnetic orderings may be varying through this region of coexistence; however, due to the high degree of peak overlap, it is difficult to reliably quantify this observation. From the temperature-dependent NPD data, we find that T_N for both commensurate and incommensurate reflections is the same.

For the $x=0.6$ sample, the NPD data were successfully modeled using a simple amplitude modulation of Mn spins directed along the *b* axis. We note that the magnetic incommensurate reflections obeyed the extinction condition $h+k=$even, and $l=$odd, which correspond to an *A* mode using the notation of Bertaut[25] and Brinks *et al.*[26] The SDW model used to successfully analyze these data was of the irreducible representation $\Gamma_3(0,A_y,0)$ [see Fig. 1(b)] and lead to a satisfactory refinements of the magnetic ordering below T_N, giving a saturated magnetic moment of $\sim 4.2\mu_B$ ($R_w(m\|b)=22.8\%$), a value slightly higher than $\sim 4.0\mu_B$ expected for Mn^{3+}. Significantly, lower quality fits to the data were obtained for models where Mn spins are collinear and point along the *a* or *c* yielding $R_w(m\|a)=24.4\%$ or $R_w(m\|c)=28.9\%$),[27] respectively. Attempts to fit a cycloidal model to these data $[\Gamma_2\times\Gamma_3(0,A_y,A_z)]$ were not statistically meaningful as powder data are incapable of uniquely differentiating between orthogonal spin components with the same extinction conditions.[26]

Using these two models for the *A*-type and SDW phases, we analyzed the NPD data in the region of coexistence with $0.4\leq x\leq 0.55$. These two models described the NPD data very well and tests also confirmed the conclusion that in both phases, the Mn moments are aligned along the *b* axis. On the $x=0.45$ sample, we tested models where the incommensurate component was placed perpendicular to k and found considerably worse fits to the data ($R_w=45\%$ and 22% for A_x and A_z incommensurate components compared to $R_w=16\%$ for the refinement of the A_y component). This result is significant as it indicates that the commensurate and incommensurate magnetic phases cannot occupy the same physical volume, as their spin components are parallel, and suggests that this intermediate region of composition between the purely *A*-type and SDW phases may be characterized by a magnetic phase separation.

We can estimate the wt % variation in the two magnetic phases across the region of coexistence by assuming that the ordered Mn moment in the region of $0.3\leq x\leq 0.45$ is the same as for the $x=0.2$ and 0.6 samples for the *A*-type and SDW phases, respectively, at 2 K. This allows us to fix the value of the ordered moment in the phase-separated region and refine the magnetic phase fraction that can be represented as wt % (Fig. 9). For the samples $x=0$, 0.1, and 0.2, we do not find any phase separation, although the ordered Mn moment we compute from the Rietveld analysis is decreasing slightly with increasing x, as does the Nd^{3+} ordered moment. These samples would represent (as deduced from the current NPD data) 100% of *A*-type phase. In the region of $0.3\leq x\leq 0.45$, the relative amount of the *A*-type phase decreases while the SDW phase replaces it and for the $x=0.6$ sample we only observe the SDW phase.

IV. DISCUSSION

From the magnetization and NPD data, we can compile the magnetic phase diagram shown in Fig. 10. In general, we find that in the $Nd_{1-x}Y_xMnO_3$ solid solution, increasing x leads to a decrease in T_N for *A*-type ordering as well as T_C for Nd^{3+} ferromagnetic ordering. The reason for this decrease is different for the two magnetic ions. The strongest influence on the Nd^{3+} ordering is the dilution of this site with nonmagnetic Y^{3+} ions. Although we cannot detect a ferromagnetic Nd component in the NPD data for $x>0.3$, our magnetization measurements suggest the presence of weak ferromagnetism for x as high as $x=0.5$, while no ferromagnetism is detected for $x=0.6$, within the sensitivity of our measurements.

The decrease in T_N for the *A*-type ordering is strongly coupled to the changes in the Mn-O-Mn angles that accompany the reduction in $\langle r_A\rangle$. Indeed, this behavior tracks well the magnetic phase diagrams established for the $RMnO_3$ (see Fig. 10)[5] and $Eu_{1-x}Y_xMnO_3$ (Ref. 21) systems and suggests that the decrease in T_N in $Nd_{1-x}Y_xMnO_3$ is due to the (aver-

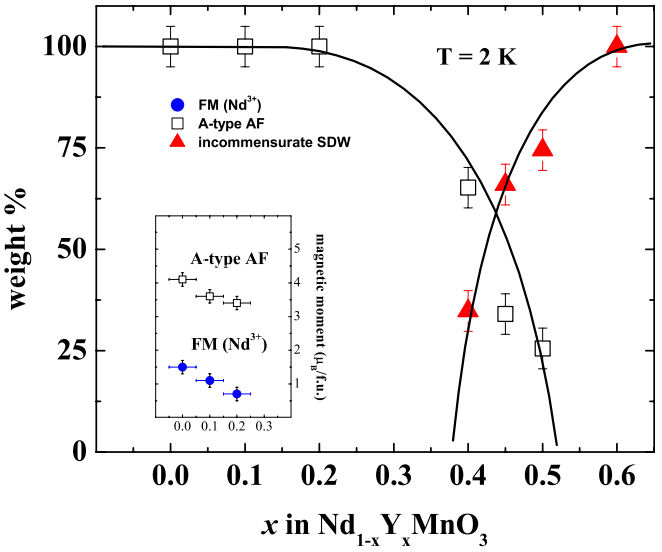

FIG. 9. (Color online) Relative amounts (in wt %) for the two magnetic phases found in the $Nd_{1-x}Y_xMnO_3$ solid solution at 2 K. Here we determine the relative amounts of these magnetic phases by assuming that in the mixed phase region, the magnetic ordering is the same as in the $x=0.2$ and 0.6 samples for the A-type and SDW phases, respectively. While the amplitude of the Mn spin remains fixed in the analysis of the $x=0.45$, 0.5, and 0.55 samples, the magnetic phase fraction is allowed to vary. For the remaining compositions where a single magnetic phase was observed, the magnetic scale factor was set to equal that of the structural nuclear scale factor. In the inset, we show the results of the size of the Nd and Mn magnetic moments determined from the Rietveld analysis of the NPD of composition with $x \leq 0.2$.

age) structural tuning of the relative strength and sign of nearest- and next-nearest magnetic interactions. The similarities between the phase diagrams of the RMnO$_3$ and $Nd_{1-x}Y_xMnO_3$ systems are not limited to the decrease in T_N.

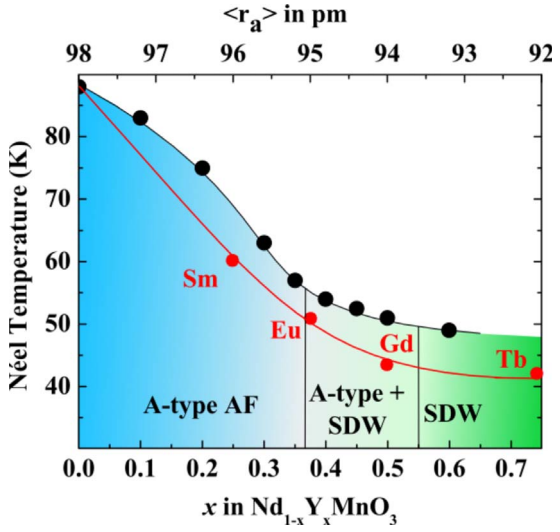

FIG. 10. (Color online) Magnetic phase diagram for the $Nd_{1-x}Y_xMnO_3$ solid solution determined from this work. The Néel temperature for the RMnO$_3$ series of manganites is also shown and is taken from Ref. 4.

The observation of a SDW magnetic ground state for higher x compositions coincides with $\langle r_A \rangle$ values similar to those for TbMnO$_3$ which exhibits SDW order below $T_N \sim 41$ K and cycloidal order below 28 K. Indeed, the direction and magnitude of the incommensurate propagation vector are very similar in the $Nd_{1-x}Y_xMnO_3$ series as found for TbMnO$_3$.[7] All these observation suggest that the variation in $\langle r_A \rangle$ tunes magnetic interactions in this solid solution in a similar way as found for the RMnO$_3$ compounds. Therefore, this system is an excellent analog of the RMnO$_3$ perovskites and facilitates the investigation of how A-type order is destabilized due to structural tuning. Of ultimate interest is the possibility of finely tuning magnetic interactions in order to investigate magnetoelectric coupling and we are currently performing appropriate measurements to asses the multiferroic properties of these materials.

One feature of the $Nd_{1-x}Y_xMnO_3$ phase diagram that differs from that of the RMnO$_3$ manganites is the observation of a magnetic phase separation between the A-type and SDW phases. Such behavior suggests that the transition between these two ground states is not continuous but rather it is separated by first-order-like phase boundaries. The observation of this phase separated region is not predicted for the RMnO$_3$ manganites based on Monte Carlo simulations.[8] One aspect of the $Nd_{1-x}Y_xMnO_3$ series that is different to the RMnO$_3$ manganites is that the size mismatch of Nd and Y is significant enough to introduce a random potential into the perovskite lattice that in turn can modulate magnetic interactions significantly on the local scale, close to the A-type to SDW phase boundary as a function of x. Such random potential or quenched disorder was discussed in phase-separation models of the colossal magnetoresistance or charge-doped manganites and it is generally regarded to lead to the phase separation at the boundary between the two competing phases:[2,28] in this case, the A-type and SDW magnetic phases. Here, the effect of small compositional fluctuations that has a large effective spatial range due to the relaxation of the lattice around them can favor one magnetic phase over the other.[29]

In summary, we have been able to synthesize $Nd_{1-x}Y_xMnO_3$ singe phase sample in the region of $0 \leq x \leq 0.6$. At low x values, we find that the ordering of Mn spins is antiferromagnetic A type, while for $x=0.6$ we find an incommensurate SDW phase as the magnetic ground state. With increasing x, the ferromagnetically ordered moment of Nd^{3+} decreases due to the dilution with nonmagnetic Y^{3+}. For intermediate compositions of $0.4 \leq x \leq 0.55$, we find a region of coexistence between the A-type and SDW magnetic ground states.

ACKNOWLEDGMENTS

We thank K. Kiefer and J. Veira for the assistance during the experiments and P. Henry and S. A. J. Kimber for critical comments during the preparation of the paper. We thank M. Steiner for helpful discussions. S.L. thanks the Deutsche Forschungsgemeinschaft for financial support under Contract No. AR 613/1-1.

*argyriou@helmholtz-berlin.de

[1] Y. Tokura, Rep. Prog. Phys. **69**, 797 (2006).
[2] E. Dagotto, T. Hotta, and A. Moreo, Phys. Rep. **344**, 1 (2001).
[3] J. Goodenough, Phys. Rev. **100**, 564 (1955).
[4] T. Kimura, S. Kawamoto, I. Yamada, M. Azuma, M. Takano, and Y. Tokura, Phys. Rev. B **67**, 180401(R) (2003).
[5] T. Kimura, S. Ishihara, H. Shintani, T. Arima, K. T. Takahashi, K. Ishizaka, and Y. Tokura, Phys. Rev. B **68**, 060403(R) (2003).
[6] J. S. Zhou and J. B. Goodenough, Phys. Rev. Lett. **96**, 247202 (2006).
[7] S. Cheong and M. Mostovoy, Nature Mater. **13**, 6 (2007).
[8] S. Dong, R. Yu, S. Yunoki, J.-M. Liu, and E. Dagotto, Phys. Rev. B **78**, 155121 (2008).
[9] A. Muñoz, M. Casáis, J. A. Alonso, M. J. Martínez-Lope, J. L. Martínez, and T. Fernández-Díaz, Inorg. Chem. **40**, 1020 (2001).
[10] T. Goto, T. Kimura, G. Lawes, A. P. Ramirez, and Y. Tokura, Phys. Rev. Lett. **92**, 257201 (2004).
[11] T. Kimura, G. Lawes, T. Goto, Y. Tokura, and A. P. Ramirez, Phys. Rev. B **71**, 224425 (2005).
[12] T. Kimura, T. Goto, H. Shintani, K. Ishizaka, T. Arima, and Y. Tokura, Nature (London) **426**, 55 (2003).
[13] N. Aliouane, D. N. Argyriou, J. Strempfer, I. Zegkinoglou, S. Landsgesell, and M. v. Zimmermann, Phys. Rev. B **73**, 020102(R) (2006).
[14] B. Lorenz, Y.-Q. Wang, and C.-W. Chu, Phys. Rev. B **76**, 104405 (2007).
[15] I. A. Sergienko and E. Dagotto, Phys. Rev. B **73**, 094434 (2006).
[16] V. Cherepanov, L. Barkhatova, A. Petrov, and V. Voronin, J. Solid State Chem. **118**, 53 (1995).
[17] H. Brinks, H. Fjellvag, and A. Kjekshus, J. Solid State Chem. **129**, 334 (1997).
[18] T. C. Hansen, P. Henry, H. Fischer, J. Torregrossa, and P. Convert, Meas. Sci. Technol. **19**, 034001 (2008).
[19] H. Rietveld, Acta Crystallogr. **22**, 151 (1967).
[20] H. Rietveld, J. Appl. Crystallogr. **2**, 65 (1969).
[21] J. Hemberger, F. Schrettle, A. Pimenov, P. Lunkenheimer, V. Y. Ivanov, A. A. Mukhin, A. M. Balbashov, and A. Loidl, Phys. Rev. B **75**, 035118 (2007).
[22] J. Hemberger, M. Brando, R. Wehn, V. Y. Ivanov, A. A. Mukhin, A. M. Balbashov, and A. Loidl, Phys. Rev. B **69**, 064418 (2004).
[23] S. Wu, C. Kuo, H. Wang, W. Li, K. Lee, J. Lynn, and R. Liu, J. Appl. Phys. **87**, 5822 (2000).
[24] A. Mukhin, V. Ivanov, V. Travkin, and A. Balbashov, J. Magn. Magn. Mater. **226-230**, 1139 (2001).
[25] E. Bertaut, J. Magn. Magn. Mater. **24**, 267 (1981).
[26] H. W. Brinks, J. Rodríguez-Carvajal, H. Fjellvåg, A. Kjekshus, and B. C. Hauback, Phys. Rev. B **63**, 094411 (2001).
[27] The higher R factors in the $x=0.6$ sample are due to the mentioned impurities in this sample.
[28] J. Burgy, M. Mayr, V. Martin-Mayor, A. Moreo, and E. Dagotto, Phys. Rev. Lett. **87**, 277202 (2001).
[29] C. Frontera and M. García-Muñoz, EPL **84**, 67011 (2008).